
Navigating the Safety-Fidelity Trade-off: Massive-Variate Time Series Forecasting for Power Systems via Probabilistic Scenarios

Kaijie Xu ZJU-UIUC Institute Zhejiang University Hangzhou, China Kaijie.23@intl.zju.edu.cn	Anqi Wang ZJU-UIUC Institute Zhejiang University Hangzhou, China anqi.23@intl.zju.edu.cn	Xilin Dai* ZJU-UIUC Institute Zhejiang University Hangzhou, China xilin2023@zju.edu.cn
---	---	---

Abstract

Probabilistic forecasting models are increasingly deployed on multivariate systems with distinct channel physics and operational constraints, but existing benchmarks evaluate neither property at scale. Public canonical multivariate benchmarks cap out at 2,000 channels, while power-system benchmarks either lack temporal structure or probabilistic evaluation. We introduce PowerPhase, a probabilistic forecasting benchmark built on six transmission grids ranging from 2,000 to 36,964 jointly forecasted channels, more than an order of magnitude beyond popular canonical multivariate benchmarks. Each target trajectory is the output of an AC power-flow solve, and PowerPhase ships with constraint-aware metrics (Safety_mBrier, NECV, CVaR $_{\alpha}$) that complement CRPS and Distortion. Across eight baselines and three seeds, distributional accuracy and constraint satisfaction rank models differently, a trade-off we term *safety-fidelity*. We further propose PowerForge, a scenario-based quantile forecaster with type-specific decoding heads and a causal bridge between variable groups, which achieves the best average rank on every grid.

1 Introduction

Multivariate time series forecasting underlies decision-making in domains as diverse as retail demand, transportation, climate, healthcare, and finance [6; 26; 3; 12]. Forecasting on power systems has become one of the most operationally consequential instances of this problem [21], because short-term predictions of grid state feed into reserve scheduling, contingency screening, and short-term market clearing [29; 51; 50]. As renewables and distributed loads push grids toward more stochastic operation [20; 54], probabilistic forecasts of grid state have moved from a research curiosity to a routine operational tool [37].

Yet forecasting on a transmission grid is more constrained than the classic multivariate setting. At every bus, an operator observes four physically coupled quantities: the active power P , the reactive power Q , the voltage magnitude V , and the voltage angle θ [15]. These quantities are tied together through the AC power flow equations [47], so a useful forecast must respect not only temporal dependencies across channels but also instantaneous physical feasibility. *This creates two difficulties that existing benchmarks and models do not address.* **First**, standard probabilistic scoring rules such as CRPS and log-likelihood average over the full forecast distribution and do not distinguish whether errors fall inside or outside the operating envelope. A model that achieves low CRPS while systematically underestimating voltage excursions can be more dangerous in practice than one with slightly worse distributional fit but reliable constraint satisfaction. **Second**, the number of channels

*Corresponding author.

grows linearly with the network, which means a moderately sized transmission system already exceeds the scale at which most public multivariate benchmarks live.

Existing public benchmarks reflect this gap. The multivariate suites commonly used in the machine learning literature, including ETT [56], Electricity, Traffic [24], and the Wikipedia Web Traffic series in the multivariate configuration of Salinas et al. [39], top out at roughly 2,000 jointly forecasted channels. None of these datasets distinguishes channels by physical role or ships with a feasibility model, so there is no standard way to measure whether a probabilistic forecast respects the physical constraints of the system it describes. The power-systems community has developed the opposite kind of artifact [8]. Tools such as pandapower [42] and the PEGASE test cases [22] expose network models with thousands of buses [28], but they are simulators rather than benchmarks. They provide neither standardized forecasting splits nor probabilistic metrics, and they are typically used without strong learning baselines. Existing bridges between the two communities cover either snapshot regression or small-scale temporal data, leaving the transmission-scale probabilistic regime unaddressed.

On the modeling side, multivariate probabilistic forecasting has progressed quickly, but largely on smaller settings. Autoregressive likelihood models such as DeepAR [40], conditioned flow models such as Transformer-TempFlow [34], diffusion approaches such as TimeGrad [35], and copula-based models such as TACTiS [14] all rely on per-step density estimation, which scales poorly when the number of channels reaches tens of thousands. A complementary line of work replaces density estimation with a small set of weighted scenarios, as in TimeMCL [9] and TimePrism [10]. This scenario-based view is well aligned with how grid operators already reason about uncertainty in terms of finite contingencies, but it has not yet been pushed to transmission scale.

We address both the benchmarking gap and the modeling gap. On the modeling side, we propose **PowerForge**, a probabilistic forecasting model whose design is driven by the constraints that transmission-scale grids impose. To evaluate PowerForge and future methods under these constraints, we release **PowerPhase**, a companion benchmark. Our contributions are:

Contributions.

- We release **PowerPhase**, a multivariate probabilistic forecasting benchmark covering six transmission networks of up to 36,964 physically typed channels, more than an order of magnitude beyond the largest canonical multivariate benchmark (Wiki, 2,000 channels), bringing the high-dimensional regime into reach of standard forecasting evaluation.
- PowerPhase introduces voltage-safety evaluation into the protocol. Each series is generated by AC power flow on perturbed load and generation profiles, and the benchmark ships with a constraint-aware metric suite (Safety_mBrier, NECV, CVaR $_{\alpha}$) that complements average-case scores such as CRPS, so models are assessed on voltage safety in addition to distributional accuracy. Evaluation across five grid sizes, three seeds, and eight baselines reveals that distributional accuracy and constraint satisfaction rank models differently, a trade-off we term *safety-fidelity*.
- We propose **PowerForge**, a scenario-based probabilistic model designed for this regime. It predicts a small set of ordered quantile scenarios that keep training and inference tractable at tens of thousands of channels. Three architectural priors drive the design: an anchor-based residual representation that removes the dominant diurnal component before encoding, type-aware decoding heads for channels with structurally different supports, and a causal cross-type bridge that encodes a known directional dependence as an architectural prior. Training uses an ordered-quantile objective with physics terms that remain tractable at the full PowerPhase scale.

2 Related Work

Multivariate probabilistic forecasting. Approaches to multivariate probabilistic forecasting differ in how they parameterize the predictive distribution [16]. DeepAR [40] learns an autoregressive parametric likelihood, deep state-space models combine recurrent latent dynamics with probabilistic emissions [33], and Salinas et al. [39] extends this idea with a low-rank Gaussian copula. Normalizing-flow variants such as TempFlow and Transformer-TempFlow [34] replace the parametric head with a conditioned flow, and TimeGrad [35] and ScoreGrad [53] parameterize the per-step conditional through denoising diffusion or score matching. Attentional copula models go further by factoring the joint distribution through an explicit copula transformer, as in TACTiS [14] and TACTiS-2 [4]. Instead, scenario-based line of work, including TimeMCL [9] and TimePrism [10], predicts a small

set of weighted hypotheses. How these approaches behave when channel numbers are in the tens of thousands remains untested.

Multivariate time series benchmarks. The methods above are typically validated on a series of public benchmarks. Commonly used datasets in time series, like ETT, Electricity, Traffic, Solar, Exchange-Rate, and Wiki datasets by Lai et al. [24]; Salinas et al. [39]; Zhou et al. [56]; Wu et al. [48] push channel counts up to roughly 2,000. Related high-dimensional forecasting work has explored global-local architectures [41], but not in transmission-scale grid-state benchmarks. Aggregated repositories such as the Monash Forecasting Archive [18], the GluonTS benchmark suite [1], and LOTSA [46] broaden coverage across domains but do not focus on per-dataset dimensionality. Meanwhile, these benchmarks have not exposed the physical structure required for probabilistic forecasters at the scale of an actual transmission grid [52].

Power-system data for machine learning. Machine learning benchmarks derived from power grids have grown rapidly [43], but each covers only part of the evaluation. **One group** supplies physical models without temporal structure [5]: PF Δ [36] benchmarks steady-state power-flow regression up to 2,000 buses, and OPFData [27] provides collections of optimal-power-flow instances. Both offer data snapshots in an independent operating point with no temporal ordering, so neither can be used for time-series evaluation. **A second group** provides temporal signals but lacks the scale or the physical evaluation that transmission grids demand. PSML [55] builds multi-scale time series from a joint transmission-distribution co-simulation on a 23-bus transmission network and 13-bus distribution feeders, focusing on cross-scale dynamics rather than the transmission-scale, bus-level probabilistic forecasting with AC-feasibility-aware evaluation considered here. Real PMU recordings aggregated through Open Power System Data [45] are partially observable and carry no feasibility ground truth. **PowerPhase is, to our knowledge, the first benchmark that combines transmission-scale channel counts, physically typed per-bus variables, temporal trajectory structure, and probabilistic evaluation with constraint-aware metrics.**

Risk-aware and constraint-aware evaluation. On the training side, risk-aware losses based on conditional value-at-risk [38] and distributionally robust objectives [31] reweight tail behaviour so that the model pays more attention to extreme outcomes, and physics-informed approaches [32; 13; 11] encode governing equations as soft regularizers to encourage physically consistent predictions. On the evaluation side, conformal prediction [2] and its time-series extensions [49] offer marginal coverage guarantees but do not measure the magnitude of constraint violations when coverage fails. Across both groups, results are reported on datasets with standard distributional metrics with limited benchmark-level assessment on how methods satisfy physical constraints.

3 The PowerPhase Benchmark

3.1 Generation Procedure

Source signals and networks. We use German TSO data from Open Power System Data [45] covering 2015 and 2016 at 15-minute resolution, retaining the aggregate load, solar generation, and wind generation series after linear interpolation of missing entries. The resulting record has 70,176 time steps. We instantiate six standard pandapower test cases [42] ranging from 500 to 9,241 buses, listed with per-network citations in Table 1.

Per-node injection synthesis. Each load bus is assigned one of five daily-shape profiles (Figure 1) and a per-node power factor; spatially correlated regional noise is added before the power-flow solve. Profile assignment rules, noise levels, and power-factor ranges are detailed in Appendix A.1.

AC power-flow solve. For every time step we run AC power flow through pandapower using Newton–Raphson with iterative back-off on the injection magnitudes until convergence. Failed steps, which account for fewer than 1% of the record on every network, are forward-filled with the last converged state. The final output for each bus is the four-vector (P, Q, V, θ) .

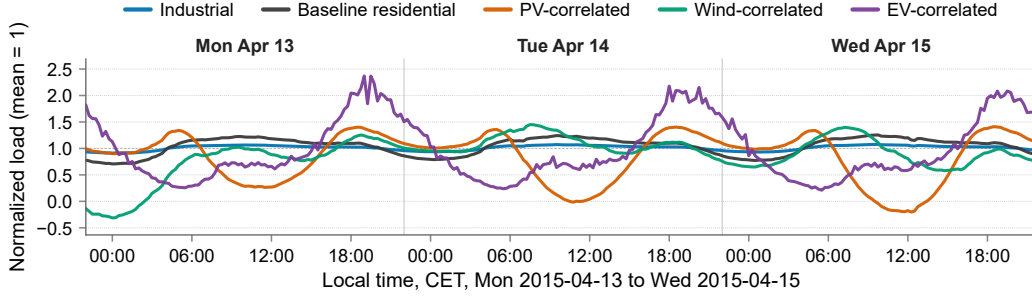


Figure 1: The five daily-shape load profiles used in the per-node injection synthesis, shown over three consecutive days in April 2015 and normalised to unit mean. Industrial profiles are nearly flat, baseline residential follows a morning-evening double peak, PV- and wind-correlated profiles track renewable availability, and EV-correlated profiles peak in the late evening. Each load bus is assigned one profile at instantiation; high-voltage buses are preferentially assigned industrial profiles.

Table 1: The six networks in PowerPhase. PQ is the number of load buses; the remaining buses are voltage-controlled (PV) or the reference bus. $Channels$ equals $4 \times buses$. $Steps$ is the total length at 15-minute resolution; $Test$ is the number of rolling-origin prediction windows per network.

Network	Buses	PQ	Channels	Steps	Pred.	Test
ACTIVSg 500 [7]	500	410	2,000	70,176	96	10
PEGASE 1354 [22]	1,354	1,094	5,416	70,176	96	10
Polish 2383 [57]	2,383	2,056	9,532	70,176	96	10
PEGASE 2869 [22]	2,869	2,359	11,476	70,176	96	10
Polish 3120 [57]	3,120	2,771	12,480	70,176	96	10
PEGASE 9241 [22]	9,241	7,796	36,964	70,176	96	10

3.2 Forecasting Task

A network with N buses produces a multivariate signal $Z_t \in \mathbb{R}^{4N}$ ordered as $[P_n, Q_n, V_n, \theta_n]_{n=1}^N$. Given a context of length $T_h = 672$, the task is to model the joint predictive distribution over $Z_{t+1:t+T_p}$ with $T_p = 96$, corresponding to a one-day horizon at 15-minute resolution. Evaluation uses rolling-origin testing with ten equally spaced prediction windows per network. Normalisation conventions for each variable type are given in Appendix A.2.

3.3 Metric Suite

We score forecasters along two axes. Statistical fidelity uses CRPS [17] averaged over channels and time, plus Distortion [9] for scenario models. Definitions and the probability-weighted CRPS variant [19] are deferred to Appendix A.3.

Operational voltage safety is evaluated on the voltage band $[V_{\min}, V_{\max}] = [0.95, 1.05]$ p.u.. For each voltage-channel evaluation point $(t, d) \in \mathcal{V}$, let $Y_{t,d} = \mathbf{1}\{V_{t,d} \notin [V_{\min}, V_{\max}]\}$ and $\hat{Y}_{t,d}^{(k)} = \mathbf{1}\{\hat{V}_{t,d}^{(k)} \notin [V_{\min}, V_{\max}]\}$. We also define the scenario violation magnitude

$$\delta_{t,d}^{(k)} = (V_{\min} - \hat{V}_{t,d}^{(k)})_+ + (\hat{V}_{t,d}^{(k)} - V_{\max})_+.$$

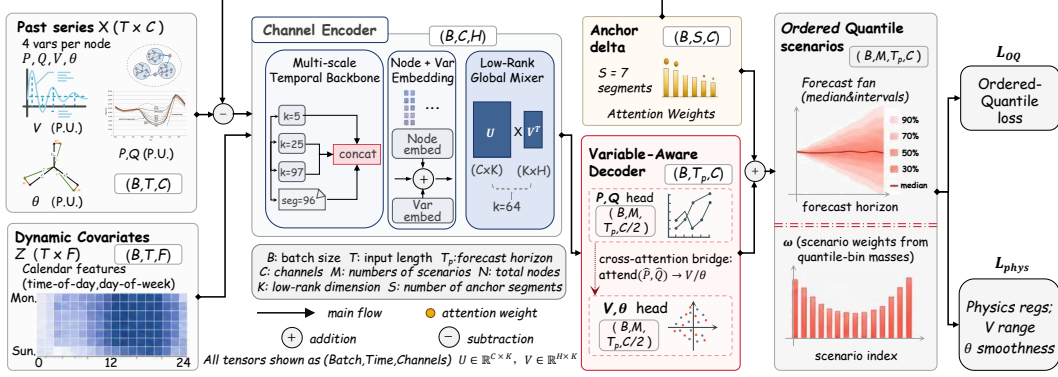


Figure 2: PowerForge architecture. The past series $X \in \mathbb{R}^{T \times C}$ is anchor-subtracted and passed through a channel encoder (multi-scale temporal backbone with kernels $\{5, 25, 97\}$, node and variable embeddings, and a low-rank global mixer). Calendar covariates Z are injected as time-aggregated context. A variable-aware decoder produces M scenario branches with separate P, Q and V, θ heads linked by a causal cross-attention bridge from \hat{P}, \hat{Q} to V, θ . The anchor is added back, and pointwise sorting along the scenario axis yields ordered quantile scenarios with quantile-bin weights ω . The model is trained with an ordered-quantile pinball loss \mathcal{L}_{OQ} and physics regularisers $\mathcal{L}_{\text{phys}}$.

For scenario weights w_k (uniform $1/K$ for sample-based methods), we report

$$\text{Safety_mBrier} = \frac{1}{|\mathcal{V}|} \sum_{(t,d) \in \mathcal{V}} \sum_k w_k (\hat{Y}_{t,d}^{(k)} - Y_{t,d})^2, \quad (1)$$

$$\text{NECV} = \frac{1}{|\mathcal{V}|} \sum_{(t,d) \in \mathcal{V}} \sum_k w_k \delta_{t,d}^{(k)}, \quad (2)$$

$$\text{CVaR}_{0.1} = \frac{1}{|\mathcal{V}|} \sum_{(t,d) \in \mathcal{V}} \frac{1}{\lceil 0.1K \rceil} \sum_{k \in \mathcal{T}_{0.1}(t,d)} \delta_{t,d}^{(k)}, \quad (3)$$

where $\mathcal{T}_{0.1}(t, d)$ contains the $\lceil 0.1K \rceil$ scenarios with the largest $\delta_{t,d}^{(k)}$. Safety_mBrier measures violation detection, whereas NECV and CVaR_{0.1} measure average and worst-decile violation severity. Additional details, including the relation to the standard Brier score [30], are given in Appendix A.3.

4 The PowerForge Model

4.1 Overview

The PowerForge architecture is shaped by three constraints of the PowerPhase regime. First, cross-variable interaction must be sub-quadratic in the channel count, since C on the larger PowerPhase grids reaches 10^4 . Second, decoding must be type-heterogeneous, since the four physical quantities have structurally different supports. Third, when the variable types carry a known directional dependence, the architecture should reflect that structure rather than discover it from gradients.

Figure 2 traces these principles through the model. The past series $X \in \mathbb{R}^{T \times C}$ is first projected into a residual space by subtracting an anchor Z^{ref} that captures the dominant diurnal pattern (§4.2). The residual is then consumed by a channel encoder and a low-rank global mixer that exchanges information across all C channels through $K \ll C$ shared tokens (§4.3). A variable-aware decoder (§4.4) emits M scenario branches through separate P, Q and V, θ heads, with a causal cross-attention bridge that conditions \hat{P}, \hat{Q} on the predicted V, θ and reflects the AC power-flow direction. Adding the anchor back and sorting along the scenario axis produces ordered quantile trajectories $\{(\hat{Z}^{(m)}, w_m)\}_{m=1}^M$. With M in the low tens, all scenarios are produced in a single forward pass, in contrast to the per-step sampling of autoregressive density baselines. Training uses an ordered-quantile pinball loss with physics regularisers (§4.5).

4.2 Reference-Anchored Residual Space

The model operates in a residual space defined relative to a learned reference $Z^{\text{ref}} \in \mathbb{R}^{L \times C}$. The reference is subtracted from the input history before encoding, and added back to the decoder output to recover absolute predictions. Working in this space removes the dominant diurnal component shared across all power-grid signals, leaving the encoder and decoder to model only the deviations.

The reference is built from the recent history. The last S daily segments of length L are extracted, and each channel forms its own reference as a per-channel attention-weighted average. Let $X_c^{(s)}$ denote the s -th segment of channel c and X_c^{query} the last Q steps of the input. Then

$$Z_c^{\text{ref}} = \sum_{s=1}^S a_{s,c} X_c^{(s)}, \quad a_{s,c} = \frac{\exp(\rho(X_c^{(s)}, X_c^{\text{query}})/\tau)}{\sum_{s'=1}^S \exp(\rho(X_c^{(s')}, X_c^{\text{query}})/\tau)}, \quad (4)$$

where ρ is the Pearson correlation between the last Q steps of $X_c^{(s)}$ and X_c^{query} , computed per channel so different channels can favour different segments. A short bias correction further aligns the reference to the most recent observations near the input boundary. Details are in Appendix B.1.

4.3 Channel Encoder and Global Token Mixer

The channel encoder (Appendix B.3) maps the residual input into a per-channel representation $h \in \mathbb{R}^{B \times C \times H}$ via a multi-scale temporal backbone with kernel sizes $\{5, 25, 97\}$ together with node, variable, and calendar embeddings. Self-attention across channels would scale as $\mathcal{O}(C^2)$, which is prohibitive at this scale [44]. We replace this dense interaction with a low-rank mixer that maintains K learnable global tokens $G \in \mathbb{R}^{K \times H}$ and alternates read and write attention. Channel states first attend to G (read), G then attends back to the updated channels (write), and a second read propagates the refreshed tokens to the channels, with the two read steps sharing projection weights. Both directions cost $\mathcal{O}(CK)$ with $K \ll C$, so the total cost is linear in C . The K tokens act as a rank- K bottleneck on cross-channel interaction, which is well matched to grids where system-wide load and renewable generation mix a handful of latent factors into thousands of channels.

4.4 Type-Aware Decoder with Cross-Type Bridge

The decoder operates in the residual space defined in §4.2, producing M hypothesis trajectories through per-type output heads and a causal cross-type bridge, instantiated on PowerPhase with $\{P, Q, V, \theta\}$.

Type-specific heads. Each channel state h_c is fused with M learnable scenario embeddings through the additive injection $h_c^{(m)} = h_c + e_m$, so the M branches differ at the embedding level before any per-type processing. A per-type head then maps each fused state to a residual prediction $\delta_c^{(m)}$, with the parameterisation chosen to match the support of each variable. The P and Q heads emit an unbounded linear projection of the fused state, with a small Gaussian perturbation added as a stochastic regulariser. The V and θ heads pass a learned projection through a tanh gate scaled by a per-type magnitude Δ_c , matching the narrow dynamic range these channels occupy after anchor subtraction. Full head equations and angular wrapping for θ are given in Appendix B.2.

Causal cross-type bridge. The AC power-flow equations determine bus voltages and angles given the active and reactive power injections [47]. The decoder reflects this direction by producing P and Q predictions first, projecting each predicted trajectory into a hidden token $\phi_c^{(u)}$ for $u \in \{P, Q\}$, and letting the V and θ hidden states attend to them through scaled dot-product attention,

$$h_c^{(m,t)} \leftarrow h_c^{(m,t)} + \gamma \cdot \text{Attn}(W_q h_c^{(m,t)}, W_k \Phi_c^{(m)}, W_v \Phi_c^{(m)}), \quad t \in \{V, \theta\}, \quad (5)$$

where $\Phi_c^{(m)} = \{\phi_c^{(P)}, \phi_c^{(Q)}\}$ collects the two source tokens, W_q, W_k, W_v are projections shared across nodes and scenarios, and γ is a scale initialised at 1. The bridge is an inductive bias rather than a hard constraint, since the projection weights can downweight the attention output when the conditioning is uninformative.

4.5 Training Objective

After the per-type heads emit residuals and the anchor is added back, the M trajectories are pointwise sorted along the scenario axis, so branch m is interpreted as the quantile estimator at level τ_m , with $\tau_1 < \dots < \tau_M$ controlled by a learnable Beta(α, β) shape. Each branch is supervised by a pinball loss at its assigned level [23],

$$\mathcal{L}_{\text{OQ}} = \frac{1}{BMT_p C} \sum_{b,m,t,c} \rho_{\tau_m}(Z_{b,t,c} - \hat{Z}_{b,t,c}^{(m)}), \quad \rho_{\tau}(u) = u(\tau - \mathbf{1}\{u < 0\}). \quad (6)$$

where B is the batch size and the sum runs over the T_p forecast steps. Four learnable per-type coefficients (one each for P, Q, V, θ) scale the per-type contributions to balance gradients across variables, initialised from inverse volatility on a small set of calibration batches. A physics regulariser dampens the voltage-residual magnitude and penalises temporal discontinuities in the angle channel. Scenario weights w_m derived from the τ_m grid (Appendix B.4) are used at evaluation in weighted CRPS, weighted Safety_mBrier, and the categorical sampler. Quantile-fan regularisers and the Beta prior are detailed in Appendix B.4.

5 Experiments

5.1 Setup

Baselines and Protocol. We compare PowerForge against eight probabilistic forecasting baselines spanning three families. *Sample-based density models:* DeepAR [40], TempFlow and Transformer-TempFlow [34], TimeGrad [35], and TACTiS-2 [4]. *Scenario-based models:* TimeMCL [9] and TimePrism [10]. *Statistical baseline:* ETS (exponential smoothing), fitted independently per channel. Every model is trained on each of the five main PowerPhase networks (ACTIVSg 500 through Polish 3120) with three random seeds, and we report the mean across seeds. At the upper end of the benchmark, PEGASE 9241 (36,964 channels) is evaluated against four baselines spanning scenario-based, conditioned-flow, and statistical families (Appendix E). Each forecasting window uses $T_h = 672$ context steps and predicts $T_p = 96$ steps ahead, evaluated through rolling-origin testing with ten windows per network. Density baselines draw $K = 100$ forecast samples at test time, and scenario-based models produce weighted hypothesis trajectories per their respective configurations (PowerForge: $M = 16$). Train, validation, and test splits are fixed across all models and seeds (Appendix C.2.2). All deep models are trained on a single NVIDIA RTX PRO 6000 Blackwell GPU with Adam, and the checkpoint with the lowest validation loss is used for evaluation. Deep baselines follow their GluonTS [1] reference configurations. ETS is fitted per channel by maximum likelihood on CPU. Full PowerForge and baseline hyperparameters are in Appendix C.2.

5.2 Main Result

Table 2 reports the four-metric scoreboard on three representative grids. The results on all five main grids are in Appendix D, and the result of PEGASE 9241 evaluation is in Appendix E. PowerForge attains the best average rank on every grid (1.2, 1.2, 1.0) and is the only model that stays in the top tier across both fidelity and Safety axes. At 500-bus, it achieves the best score on all four metrics, with Safety_mBrier and CVaR_{0.1} tied at 0 alongside TACTiS-2. At 2383-bus, PowerForge matches TACTiS-2 on CRPS within one standard deviation, while attaining the best Distortion and the lowest Safety_mBrier (0.0010, vs. 0.0032 for TempFlow and Transformer-TempFlow) and CVaR_{0.1}. At 3120-bus, it is strict best on every metric, with a Distortion more than $2\times$ lower than the next baseline.

The table makes the safety–fidelity trade-off concrete. TimePrism is the clearest instance, with a competitive CRPS at 2383-bus (0.0096) but the largest CVaR_{0.1} (3.50) of any deep baseline, indicating that the winner-takes-all training criterion produces low-probability hypotheses that drift far outside the operational band. TimeMCL shows a milder version of the same pattern at 500-bus, where strong CRPS (0.0054) coexists with mediocre CVaR_{0.1} (0.19). DeepAR fails on both axes, with the worst CRPS on every grid and Safety_mBrier never below 0.54. Density-based models behave inconsistently across scales. TACTiS-2 wins or ties on 500-bus security but its Safety_mBrier rises from 0 to 0.04 at 3120-bus. TempFlow and Transformer-TempFlow show the inverse trend, weak on 500-bus security but reaching the second-best tier on 3120-bus. ETS, despite its simplicity, is surprisingly strong at small scale and degrades steadily with channel count. No baseline holds a stable

Table 2: Probabilistic forecasting results on POWERPHASE (three representative grids; full results in Appendix D). CRPS and Distortion measure *fidelity*; Safety_mBrier and CVaR_{0.1} measure *safety*. All values are mean \pm std over three seeds. **Bold**: best; underline: second best. *Rank* is the model’s average rank within the grid across the four metrics.

Grid	Model	Fidelity \downarrow		Safety \downarrow		Rank
		CRPS	Distortion	Safety_mBrier	CVaR _{0.1}	
500-bus	DeepAR	0.1156 \pm .0240	0.5537 \pm .1310	0.9519 \pm .0233	2.1753 \pm .6901	8.8
	ETS	0.0064 \pm .0000	0.0481 \pm .0000	0.0561 \pm .0002	<u>0.0116</u> \pm .0000	4.2
	TimeMCL	<u>0.0054</u> \pm .0003	<u>0.0118</u> \pm .0001	<u>0.0200</u> \pm .0200	0.1906 \pm .1907	3.2
	TimePrism	0.0077 \pm .0003	0.0195 \pm .0023	0.0221 \pm .0062	2.9950 \pm 1.1445	5.5
	TACTiS-2	0.0057 \pm .0002	0.0139 \pm .0006	0.0000 \pm .0000	0.0000 \pm .0000	<u>2.2</u>
	TempFlow	0.0144 \pm .0008	0.0679 \pm .0005	0.2740 \pm .0519	0.0332 \pm .0043	5.5
	Trans-TempFlow	0.0146 \pm .0006	0.0702 \pm .0011	0.2896 \pm .0581	0.0380 \pm .0100	6.5
	TimeGrad	0.0160 \pm .0011	0.0954 \pm .0092	0.7630 \pm .0192	0.3316 \pm .0358	7.8
	PowerForge (Ours)	0.0030 \pm .0008	0.0072 \pm .0019	0.0000 \pm .0000	0.0000 \pm .0000	1.2
2383-bus	DeepAR	0.0583 \pm .0261	0.4124 \pm .1674	0.5440 \pm .1632	0.1831 \pm .1303	8.2
	ETS	0.0111 \pm .0000	0.1513 \pm .0000	0.0352 \pm .0001	0.0099 \pm .0000	6.5
	TimeMCL	0.0070 \pm .0008	<u>0.0147</u> \pm .0016	0.0109 \pm .0068	0.0322 \pm .0547	4.5
	TimePrism	0.0096 \pm .0085	0.0250 \pm .0164	0.0294 \pm .0255	3.5007 \pm 1.1821	6.8
	TACTiS-2	0.0039 \pm .0000	0.0188 \pm .0000	0.0036 \pm .0000	0.0007 \pm .0000	3.5
	TempFlow	0.0057 \pm .0001	0.0153 \pm .0026	<u>0.0032</u> \pm .0001	<u>0.0005</u> \pm .0000	<u>2.8</u>
	Trans-TempFlow	0.0060 \pm .0002	0.0174 \pm .0002	<u>0.0032</u> \pm .0000	<u>0.0005</u> \pm .0000	3.2
	TimeGrad	0.0169 \pm .0016	0.1753 \pm .0826	0.5454 \pm .0505	0.8028 \pm .4729	8.2
	PowerForge (Ours)	<u>0.0042</u> \pm .0019	0.0084 \pm .0025	0.0010 \pm .0002	0.0004 \pm .0000	1.2
3120-bus	DeepAR	0.1408 \pm .0148	0.7666 \pm .0842	0.7883 \pm .0160	1.6903 \pm .5156	8.8
	ETS	0.0180 \pm .0001	0.1954 \pm .0000	0.0987 \pm .0001	0.0225 \pm .0000	6.8
	TimeMCL	0.0092 \pm .0052	<u>0.0162</u> \pm .0044	0.1100 \pm .1071	0.2240 \pm .2385	5.2
	TimePrism	0.0083 \pm .0018	0.0213 \pm .0119	0.0579 \pm .0383	5.4230 \pm 3.2742	6.0
	TACTiS-2	<u>0.0043</u> \pm .0000	0.0297 \pm .0001	0.0428 \pm .0006	0.0071 \pm .0000	4.0
	TempFlow	0.0055 \pm .0001	0.0178 \pm .0001	0.0187 \pm .0000	0.0035 \pm .0000	3.5
	Trans-TempFlow	0.0054 \pm .0002	0.0175 \pm .0006	<u>0.0184</u> \pm .0004	<u>0.0034</u> \pm .0000	<u>2.5</u>
	TimeGrad	0.0123 \pm .0069	0.1295 \pm .0503	0.4234 \pm .1359	0.5695 \pm .2468	7.2
	PowerForge (Ours)	0.0038 \pm .0011	0.0076 \pm .0010	0.0068 \pm .0000	0.0025 \pm .0000	1.0

position across both scales and axes, whereas PowerForge maintains a top-tier position throughout. At PEGASE 9241 (36,964 channels), PowerForge is still best on every metric (Appendix E).

5.3 Qualitative Analysis

Figure 3 compares scenario forecasts from PowerForge, TimePrism, and TACTiS-2 on a voltage channel of Polish 2383 across three test windows. PowerForge produces a compact set of hypotheses that track the diurnal shape across all windows, with probability mass aligned to the daily pattern. TimePrism recovers the overall shape but with a wider spread, and several low-probability hypotheses visibly undershoot the evening trough. Its winner-takes-all objective rewards hypothesis diversity, so the spread is partly by design. On this channel, the diversity translates into systematic underestimation rather than informative uncertainty. TACTiS-2 shows a different failure. Its median tracks the contextual mean reasonably well but flattens through the diurnal trough, while individual samples exhibit pronounced high-frequency jitter without coherent low-frequency motion, consistent with an autoregressive copula sampler that captures per-step marginals but attenuates temporal dependence over the 96-step horizon at this channel count. These behaviours align with the metric ordering in Table 2. Producing a structured set of trajectories that respects the low-frequency physics of the system remains the harder requirement for high-dimensional grid forecasting. Additional cross-grid trajectories and aggregate bus-level distributions are reported in Appendix F.

5.4 Ablation Study

We isolate the contribution of each PowerForge component by training six ablated variants on PEGASE 1354 with all remaining hyperparameters fixed. Each variant disables a single architectural

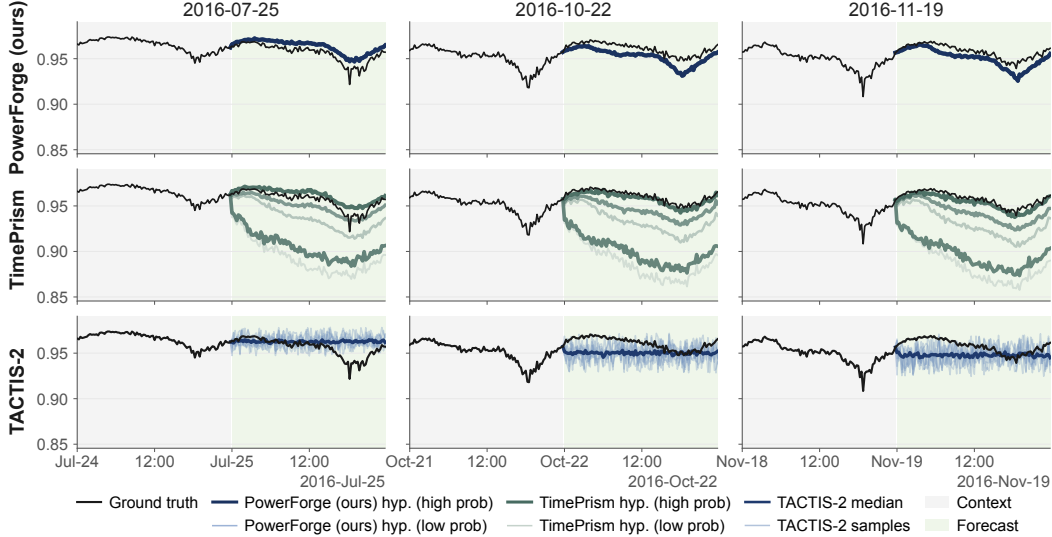


Figure 3: Voltage forecasts on Polish 2383 (9,532 channels) across three test windows. PowerForge (top) produces a compact hypothesis fan tracking the diurnal pattern. TimePrism (middle) recovers the shape with wider spread. TACTIS-2 (bottom) flattens the daily cycle under per-step sample jitter.

Table 3: Ablation on PEGASE 1354 (single seed). Δ is the relative CRPS change against the full configuration, ordered by descending impact. CRPS and Distortion measure fidelity. Lower is better for both metrics. Full safety metrics are in Appendix G.

Variant	CRPS ↓	Δ	Distortion ↓
Full PowerForge	0.0043	–	0.0110
– anchor–delta parameterisation	0.0080	+84%	0.0229
– quantile regularisation	0.0059	+37%	0.0128
– ordered-quantile loss (use WTA)	0.0055	+27%	0.0155
– physics regularisation	0.0055	+27%	0.0120
– cross-type causal bridge	0.0053	+22%	0.0120
– low-rank global token mixer	0.0045	+4%	0.0154

element or training signal. Table 3 reports CRPS and Distortion together with the relative CRPS change against the full configuration, ordered by descending impact. The anchor–delta voltage parameterisation is the single most important component. Removing it raises CRPS by 84% and Distortion by more than $2\times$, confirming that operating in residual voltage space is essential when channels span the narrow physical band around 1.0 p.u. The next tier is calibration and training signal. The quantile-fan regularisation contributes +37% CRPS, replacing the ordered-quantile criterion with winner-takes-all training contributes +27%, and removing physics regularisation contributes +27%. The cross-type causal bridge has smaller direct impact at this scale (+22%). The low-rank global mixer has the smallest CRPS impact (+4%), but its effect on Distortion is substantial (+40%, $0.0110 \rightarrow 0.0154$), indicating its role in single-best-hypothesis quality rather than overall distributional fit.

6 Conclusion and Limitations

Conclusion. We introduced PowerPhase, a probabilistic forecasting benchmark that brings transmission-scale multivariate systems into reach of evaluation, and PowerForge, an ordered-quantile scenario forecaster designed for this regime. PowerPhase ships with physically typed channels, AC-power-flow-simulated trajectories, and a voltage-risk-aware metric suite that complements scoring rules. PowerForge combines a reference-anchored residual parameterisation, type-specific decoding heads coupled through a causal cross-attention bridge, and a low-rank global mixer that exchanges information across channels through $K \ll C$ shared tokens at $O(CK)$ cost. Across the five main

grids and three seeds, it attains the best score on 19 of 20 grid-metric cells, ties with the strongest baseline on the remaining one within seed variance, and ranks first on average on every grid. The benchmark also surfaces a safety-fidelity trade-off: distributional accuracy and constraint satisfaction rank models differently, so no single average-case score is sufficient for constraint-bound decisions.

Limitations. PowerPhase evaluates voltage-band risk rather than full AC feasibility. While target trajectories are produced by AC power-flow solves, the proposed safety metrics only measure violations of the $[0.95, 1.05]$ p.u. voltage-magnitude band; they do not certify line limits, generator reactive limits, power-balance residuals, angle consistency, or feasibility of each predicted (P, Q, V, θ) scenario. The benchmark is also synthetic, driven by national load and renewable traces, archetypal bus profiles, Gaussian perturbations, and fixed power factors, so some safety-fidelity trends may reflect this simulator family. PowerForge encodes variable type and a $P, Q \rightarrow V, \theta$ dependency, but not explicit topology or admittance structure. Real-data validation, richer physical metrics, topology-aware models, and broader large-scale baseline sweeps are left for future work.

References

- [1] Alexander Alexandrov, Konstantinos Benidis, Michael Bohlke-Schneider, Valentin Flunkert, Jan Gasthaus, Tim Januschowski, Danielle C Maddix, Syama Rangapuram, David Salinas, Jasper Schulz, et al. Gluonts: Probabilistic and neural time series modeling in python. *Journal of Machine Learning Research*, 21(116):1–6, 2020.
- [2] Anastasios N. Angelopoulos and Stephen Bates. A gentle introduction to conformal prediction and distribution-free uncertainty quantification. *CoRR*, abs/2107.07511, 2021. URL <https://arxiv.org/abs/2107.07511>.
- [3] Abdul Fatir Ansari, Oleksandr Shchur, Jaris Küken, Andreas Auer, Boran Han, Pedro Mercado, Syama Sundar Rangapuram, Huibin Shen, Lorenzo Stella, Xiyuan Zhang, Mononito Goswami, Shubham Kapoor, Danielle C. Maddix, Pablo Guerron, Tony Hu, Junming Yin, Nick Erickson, Prateek Mutalik Desai, Hao Wang, Huzefa Rangwala, George Karypis, Yuyang Wang, and Michael Bohlke-Schneider. Chronos-2: From univariate to universal forecasting, 2025. URL <https://arxiv.org/abs/2510.15821>.
- [4] Arjun Ashok, Étienne Marcotte, Valentina Zantedeschi, Nicolas Chapados, and Alexandre Drouin. Tactis-2: Better, faster, simpler attentional copulas for multivariate time series. *arXiv preprint arXiv:2310.01327*, 2023.
- [5] Sogol Babaeinejadsarookolae, Adam Birchfield, Richard D Christie, Carleton Coffrin, Christopher DeMarco, Ruisheng Diao, Michael Ferris, Stephane Fliscounakis, Scott Greene, Renke Huang, et al. The power grid library for benchmarking ac optimal power flow algorithms. *arXiv preprint arXiv:1908.02788*, 2019.
- [6] Konstantinos Benidis, Syama Sundar Rangapuram, Valentin Flunkert, Yuyang Wang, Danielle Maddix, Caner Turkmen, Jan Gasthaus, Michael Bohlke-Schneider, David Salinas, Lorenzo Stella, et al. Deep learning for time series forecasting: Tutorial and literature survey. *ACM Computing Surveys*, 55(6):1–36, 2022.
- [7] Adam B Birchfield, Ti Xu, Kathleen M Gegner, Komal S Shetye, and Thomas J Overbye. Grid structural characteristics as validation criteria for synthetic networks. *IEEE Transactions on power systems*, 32(4):3258–3265, 2016.
- [8] David P Chassin, Jason C Fuller, and Ned Djilali. Gridlab-d: an agent-based simulation framework for smart grids. *Journal of Applied Mathematics*, 2014(1):492320, 2014.
- [9] Adrien Cortes, Remi Rehm, and Victor Letzelter. Winner-takes-all for multivariate probabilistic time series forecasting. In *Forty-second International Conference on Machine Learning*, 2025. URL <https://openreview.net/forum?id=4QcFfTu6UT>.
- [10] Xilin Dai, Zhijian Xu, Wanxu Cai, and Qiang Xu. From Samples to Scenarios: A New Paradigm for Probabilistic Forecasting. In *The Fourteenth International Conference on Learning Representations*, October 2025.

- [11] Xilin Dai, Ruidi Zhou, Jinhao Zhang, Keyi He, Fanfan Lin, and Hao Ma. SocNet: A Physics-Guided Neural Network for Battery State-of-Charge Estimation Robust to Temperature Variations and Sensor Noises. *IEEE Transactions on Transportation Electrification*, 11(5):11165–11176, October 2025.
- [12] Xilin Dai, Wanxu Cai, Zhijian Xu, and Qiang Xu. Position: Universal time series foundation models rest on a category error, 2026. URL <https://arxiv.org/abs/2602.05287>.
- [13] Xilin Dai, Ruidi Zhou, Jinhao Zhang, Fanfan Lin, Weifeng Zhang, and Hao Ma. Socgate: Physics-gated neural network for stable multicycle estimation of battery state-of-charge. *IEEE Transactions on Industrial Electronics*, 73(4):5518–5529, 2026. doi: 10.1109/TIE.2025.3626581.
- [14] Alexandre Drouin, Étienne Marcotte, and Nicolas Chapados. Tactis: Transformer-attentional copulas for time series. In *International Conference on Machine Learning*, pages 5447–5493. PMLR, 2022.
- [15] J Duncan Glover, Mulukutla S Sarma, Thomas Jeffrey Overbye, and NP Padhy. *Power system analysis and design*, volume 2008. Cengage Learning Stamford, CT, USA, 2012.
- [16] Tilmann Gneiting and Matthias Katzfuss. Probabilistic forecasting. *Annual Review of Statistics and Its Application*, 1(1):125–151, 2014.
- [17] Tilmann Gneiting and Adrian E Raftery. Strictly proper scoring rules, prediction, and estimation. *Journal of the American statistical Association*, 102(477):359–378, 2007.
- [18] Rakshitha Godahewa, Christoph Bergmeir, Geoffrey I Webb, Rob J Hyndman, and Pablo Montero-Manso. Monash time series forecasting archive. *arXiv preprint arXiv:2105.06643*, 2021.
- [19] Hans Hersbach. Decomposition of the continuous ranked probability score for ensemble prediction systems. *Weather and Forecasting*, 15(5):559–570, 2000.
- [20] Tao Hong and Shu Fan. Probabilistic electric load forecasting: A tutorial review. *International Journal of Forecasting*, 32(3):914–938, 2016.
- [21] Tao Hong, Pierre Pinson, Yi Wang, Rafał Weron, Dazhi Yang, and Hamidreza Zareipour. Energy forecasting: A review and outlook. *IEEE Open Access Journal of Power and Energy*, 7:376–388, 2020.
- [22] Cédric Jozs, Stéphane Fliscounakis, Jean Maeght, and Patrick Panciatici. Ac power flow data in matpower and qcqp format: itesla, rte snapshots, and pegase. *arXiv preprint arXiv:1603.01533*, 2016.
- [23] Roger Koenker and Gilbert Bassett Jr. Regression quantiles. *Econometrica: journal of the Econometric Society*, pages 33–50, 1978.
- [24] Guokun Lai, Wei-Cheng Chang, Yiming Yang, and Hanxiao Liu. Modeling long-and short-term temporal patterns with deep neural networks. In *The 41st international ACM SIGIR conference on research & development in information retrieval*, pages 95–104, 2018.
- [25] Stefan Lee, Senthil Purushwalkam Shiva Prakash, Michael Cogswell, Viresh Ranjan, David Crandall, and Dhruv Batra. Stochastic multiple choice learning for training diverse deep ensembles. *Advances in Neural Information Processing Systems*, 29, 2016.
- [26] Yiding Liu, Yifan Hu, Hongjie Xia, Peiyuan Liu, Hongzhou Chen, Xilin Dai, Zewei Dong, and Jiang-Ming Yang. Falcon-x: A time series foundation model for heterogeneous multivariate modeling, 2026. URL <https://arxiv.org/abs/2605.27286>.
- [27] Sean Lovett, Miha Zgubic, Sofia Liguori, Sephora Madjiheurem, Hamish Tomlinson, Sophie Elster, Chris Apps, Sims Witherspoon, and Luis Piloto. Opfdata: Large-scale datasets for ac optimal power flow with topological perturbations. *arXiv preprint arXiv:2406.07234*, 2024.

- [28] Steffen Meinecke, Džanan Sarajlić, Simon Ruben Drauz, Annika Klettke, Lars-Peter Lauen, Christian Rehtanz, Albert Moser, and Martin Braun. Simbench—a benchmark dataset of electric power systems to compare innovative solutions based on power flow analysis. *Energies*, 13(12): 3290, 2020.
- [29] Juan M Morales, Antonio J Conejo, Henrik Madsen, Pierre Pinson, and Marco Zugno. *Integrating renewables in electricity markets: operational problems*. Springer Science & Business Media, 2013.
- [30] Allan H Murphy. A new vector partition of the probability score. *Journal of Applied Meteorology and Climatology*, 12(4):595–600, 1973.
- [31] Hamed Rahimian and Sanjay Mehrotra. Distributionally robust optimization: A review. *arXiv preprint arXiv:1908.05659*, 2019.
- [32] Maziar Raissi, Paris Perdikaris, and George E Karniadakis. Physics-informed neural networks: A deep learning framework for solving forward and inverse problems involving nonlinear partial differential equations. *Journal of Computational physics*, 378:686–707, 2019.
- [33] Syama Sundar Rangapuram, Matthias W Seeger, Jan Gasthaus, Lorenzo Stella, Yuyang Wang, and Tim Januschowski. Deep state space models for time series forecasting. *Advances in neural information processing systems*, 31, 2018.
- [34] Kashif Rasul, Abdul-Saboor Sheikh, Ingmar Schuster, Urs Bergmann, and Roland Vollgraf. Multivariate probabilistic time series forecasting via conditioned normalizing flows. *arXiv preprint arXiv:2002.06103*, 2020.
- [35] Kashif Rasul, Calvin Seward, Ingmar Schuster, and Roland Vollgraf. Autoregressive denoising diffusion models for multivariate probabilistic time series forecasting. In *International conference on machine learning*, pages 8857–8868. PMLR, 2021.
- [36] Ana K. Rivera, Anvita Bhagavathula, Alvaro Carbonero, and Priya Donti. Pfδ: A benchmark dataset for power flow under load, generation, and topology variations, 2026. URL <https://arxiv.org/abs/2510.22048>.
- [37] Line A Roald, David Pozo, Anthony Papavasiliou, Daniel K Molzahn, Jalal Kazempour, and Antonio Conejo. Power systems optimization under uncertainty: A review of methods and applications. *Electric Power Systems Research*, 214:108725, 2023.
- [38] R Tyrrell Rockafellar, Stanislav Uryasev, et al. Optimization of conditional value-at-risk. *Journal of risk*, 2:21–42, 2000.
- [39] David Salinas, Michael Bohlke-Schneider, Laurent Callot, Roberto Medico, and Jan Gasthaus. High-dimensional multivariate forecasting with low-rank gaussian copula processes. *Advances in neural information processing systems*, 32, 2019.
- [40] David Salinas, Valentin Flunkert, Jan Gasthaus, and Tim Januschowski. Deepar: Probabilistic forecasting with autoregressive recurrent networks. *International journal of forecasting*, 36(3): 1181–1191, 2020.
- [41] Rajat Sen, Hsiang-Fu Yu, and Inderjit S Dhillon. Think globally, act locally: A deep neural network approach to high-dimensional time series forecasting. *Advances in neural information processing systems*, 32, 2019.
- [42] Leon Thurner, Alexander Scheidler, Florian Schäfer, Jan-Hendrik Menke, Julian Dollichon, Friederike Meier, Steffen Meinecke, and Martin Braun. pandapower—an open-source python tool for convenient modeling, analysis, and optimization of electric power systems. *IEEE Transactions on Power Systems*, 33(6):6510–6521, 2018.
- [43] Anna Varbella, Kenza Amara, Blazhe Gjorgiev, Mennatallah El-Assady, and Giovanni Sansavini. Powergraph: A power grid benchmark dataset for graph neural networks. In *The Thirty-eight Conference on Neural Information Processing Systems Datasets and Benchmarks Track*, 2024. URL <https://openreview.net/forum?id=qWTfC04HvT>.

- [44] Sinong Wang, Belinda Z Li, Madian Khabsa, Han Fang, and Hao Ma. Linformer: Self-attention with linear complexity. *arXiv preprint arXiv:2006.04768*, 2020.
- [45] Frauke Wiese, Ingmar Schlecht, Wolf-Dieter Bunke, Clemens Gerbaulet, Lion Hirth, Martin Jahn, Friedrich Kunz, Casimir Lorenz, Jonathan Mühlenpfordt, Juliane Reimann, et al. Open power system data—frictionless data for electricity system modelling. *Applied Energy*, 236: 401–409, 2019.
- [46] Gerald Woo, Chenghao Liu, Akshat Kumar, Caiming Xiong, Silvio Savarese, and Doyen Sahoo. Unified training of universal time series forecasting transformers. In *Forty-first International Conference on Machine Learning*, 2024.
- [47] Allen J Wood, Bruce F Wollenberg, and Gerald B Sheblé. *Power generation, operation, and control*. John wiley & sons, 2013.
- [48] Haixu Wu, Jiehui Xu, Jianmin Wang, and Mingsheng Long. Autoformer: Decomposition transformers with auto-correlation for long-term series forecasting. *Advances in neural information processing systems*, 34:22419–22430, 2021.
- [49] Chen Xu and Yao Xie. Sequential predictive conformal inference for time series. In *International Conference on Machine Learning*, pages 38707–38727. PMLR, 2023.
- [50] Kaijie Xu, Xilin Dai, and Lin Qiu. Opformer: Real-time optimal power flow with cnn-based transformer. In *ICASSP 2025 - 2025 IEEE International Conference on Acoustics, Speech and Signal Processing (ICASSP)*, pages 1–5, 2025. doi: 10.1109/ICASSP49660.2025.10888727.
- [51] Kaijie Xu, Lin Qiu, Xilin Dai, Yi Ding, Chengjin Ye, and Youtong Fang. Optimal power flow under varying topologies via physics-guided neural network with stack-learning. *International Journal of Electrical Power & Energy Systems*, 173:111391, 2025.
- [52] Zhijian Xu, Wanxu Cai, Xilin Dai, Zhaorong Deng, and Qiang Xu. Fidel-ts: A high-fidelity multimodal benchmark for time series forecasting, 2026. URL <https://arxiv.org/abs/2509.24789>.
- [53] Tijin Yan, Hongwei Zhang, Tong Zhou, Yufeng Zhan, and Yuanqing Xia. Scoregrad: Multivariate probabilistic time series forecasting with continuous energy-based generative models. *arXiv preprint arXiv:2106.10121*, 2021.
- [54] Xiaochen Zhang, Kaijie Xu, Shengchen Liao, Lin Qiu, Chengjin Ye, and Youtong Fang. Disturbed security-constrained and time-variant optimal power flow for dynamic power system based on chaotic-genetic-centroid puffin optimization. *Applied Energy*, 397:126287, 2025.
- [55] Xiangtian Zheng, Nan Xu, Loc Trinh, Dongqi Wu, Tong Huang, S Sivaranjani, Yan Liu, and Le Xie. A multi-scale time-series dataset with benchmark for machine learning in decarbonized energy grids. *Scientific Data*, 9(1):359, 2022.
- [56] Haoyi Zhou, Shanghang Zhang, Jieqi Peng, Shuai Zhang, Jianxin Li, Hui Xiong, and Wancai Zhang. Informer: Beyond efficient transformer for long sequence time-series forecasting. In *Proceedings of the AAAI conference on artificial intelligence*, volume 35, pages 11106–11115, 2021.
- [57] Ray Daniel Zimmerman, Carlos Edmundo Murillo-Sánchez, and Robert John Thomas. Matpower: Steady-state operations, planning, and analysis tools for power systems research and education. *IEEE Transactions on power systems*, 26(1):12–19, 2010.

Appendix

A	Benchmark Details	15
A.1	Data Generation Pipeline Details	15
A.1.1	Source Signals and Load Archetypes	15
A.1.2	Noise Model	15
A.1.3	Reactive Power and AC Power-Flow Solve	15
A.2	Normalisation Conventions	15
A.3	Metric Definitions	16
A.3.1	CRPS	16
A.3.2	Distortion	16
A.3.3	Voltage Safety Metrics	16
A.4	Bus Type Convention	17
A.5	Train / Validation / Test Splits	17
B	PowerForge Architecture	17
B.1	Anchor-Delta Details	17
B.2	Type-Specific Heads	18
B.3	Channel Encoder	18
B.4	Training Objective Details	19
B.4.1	Full Loss Formulation	19
B.4.2	Ordered-Quantile Loss (\mathcal{L}_{OQ})	19
B.4.3	Physics Regularisation ($\mathcal{L}_{\text{phys}}$)	19
B.4.4	Auxiliary Regularisers	19
C	Training and Implementation	19
C.1	Hyperparameters	19
C.2	Implementation Details	20
C.2.1	Per-Network Batch Size	20
C.2.2	Train, Validation, and Test Splits	20
C.2.3	Optimisation and Checkpointing	21
C.2.4	Baseline Configurations	21
D	Full Results on the Five Main Grids	22
E	Evaluation at 36,964 Channels: PEGASE 9241	22
F	Additional Safety Analyses	22
F.1	Additional Qualitative Comparison: PEGASE 1354	22
F.2	Bus-level aggregate distribution on Polish 2383	23
G	Full Ablation Results on PEGASE 1354	24

A Benchmark Details

A.1 Data Generation Pipeline Details

A.1.1 Source Signals and Load Archetypes

All PowerPhase networks are driven by three national-level seed signals from the Open Power System Data archive [45]: aggregate German load (DE_load_actual_entsoe_transparency), solar generation (DE_solar_generation_actual), and wind generation (DE_wind_generation_actual). We retain 2015–2016 at 15-minute resolution and fill missing entries by linear interpolation followed by forward and backward fill, yielding 70,176 time steps per signal.

Each load bus is classified as *high-voltage* (HV) if its nominal voltage exceeds 110 kV or its nominal active power exceeds 10 MW, and as *low-voltage* (LV) otherwise. Five normalised daily-shape profiles are constructed from the seed signals:

1. **Baseline:** the national load curve, normalised to unit mean.
2. **Industrial:** a flattened version of the national load, $\mu + \alpha_{\text{ind}}(L_t - \mu)$ with $\alpha_{\text{ind}} = 0.3$, normalised to unit mean.
3. **PV-correlated:** national load minus $k_{\text{pv}} \cdot \text{solar}$ with $k_{\text{pv}} = 3.0$, normalised to unit mean.
4. **Wind-correlated:** national load minus $k_{\text{wind}} \cdot \text{wind}$ with $k_{\text{wind}} = 2.0$, normalised to unit mean.
5. **EV-correlated:** the baseline profile boosted by +40% during 18:00–22:00, normalised to unit mean.

Each HV bus is assigned the Industrial profile with probability 0.8 and the Baseline profile with probability 0.2. Each LV bus draws from {Baseline, PV, EV, Wind} with base weights (0.4, 0.3, 0.2, 0.1), modulated by a deterministic region index $r = \text{bus_id} \bmod 3$: region 0 doubles the PV weight and region 1 doubles the Wind weight, with weights renormalised before sampling.

A.1.2 Noise Model

The per-bus active power injection at time step t is

$$P_{n,t} = P_n^{\text{nom}} \cdot s_{n,t} \cdot (1 + \varepsilon_{r(n),t}^{\text{reg}} + \varepsilon_{n,t}^{\text{node}}), \quad (7)$$

where $s_{n,t}$ is the normalised archetype shape, $\varepsilon_{r,t}^{\text{reg}} \sim \mathcal{N}(0, \sigma_{\text{reg}})$ is a spatially correlated regional noise term shared across all buses with region index $r(n)$, and $\varepsilon_{n,t}^{\text{node}} \sim \mathcal{N}(0, \sigma_n)$ is independent per-node noise. Negative injections are clipped to zero. Standard deviations are $\sigma_{\text{reg}} = 0.03$, $\sigma_n = 0.02$ for HV nodes, and $\sigma_n = 0.08$ for LV nodes.

A.1.3 Reactive Power and AC Power-Flow Solve

Reactive power is derived from active power via a per-bus power factor $\cos \phi_n$ sampled uniformly at initialisation and held fixed across all time steps,

$$Q_{n,t} = P_{n,t} \cdot \tan(\arccos(\cos \phi_n)), \quad (8)$$

with $\cos \phi_n \in [0.96, 0.99]$ for HV buses and $[0.90, 0.99]$ for LV buses.

For every time step we run AC power flow through pandapower [42] using Newton–Raphson. A magnitude back-off and an Iwamoto multiplier fallback are applied when Newton–Raphson fails to converge, and any remaining failed steps are forward-filled with the last converged state. Convergence rates exceed 99% on every PowerPhase network. Several PEGASE test cases contain generators with numerically zero $Q_{\text{max}} - Q_{\text{min}}$ ranges, which we widen to 5000 MVar before running the pipeline to avoid division-by-zero in the solver.

A.2 Normalisation Conventions

The four variable types are normalised independently before computing all evaluation metrics:

Variable	Unit	Normalisation
P (active power)	MW	divided by training-set $\max P $
Q (reactive power)	MVAr	divided by training-set $\max Q $
V (voltage magnitude)	p.u.	kept as-is
θ (voltage angle)	rad	kept as-is (converted from degrees)

The max-abs constants for P and Q are computed on the training split only and reused on validation and test, so no information from the evaluation period leaks into normalisation.

A.3 Metric Definitions

Throughout this section, let $Z \in \mathbb{R}^{B \times T \times D}$ be the ground-truth tensor over B prediction windows, T forecast steps, and D channels. A forecaster produces K scenarios $\hat{Z}^{(k)}$ with weights $w^{(k)}$ satisfying $\sum_k w_{b,d}^{(k)} = 1$. For sample-based methods, $w^{(k)} = 1/K$ uniformly.

A.3.1 CRPS

We compute CRPS via the energy-score representation,

$$\text{CRPS}_{b,t,d} = \sum_k w_{b,d}^{(k)} |\hat{Z}_{b,t,d}^{(k)} - Z_{b,t,d}| - \frac{1}{2} \mathbb{E}_w [|\hat{Z} - \hat{Z}'|], \quad (9)$$

and exploit the sorted-CDF identity for efficient computation of the second term. With scenarios sorted in ascending order $\hat{Z}^{(\pi_1)} \leq \hat{Z}^{(\pi_2)} \leq \dots$ and cumulative weights $F_i = \sum_{j=1}^i w_{b,d}^{(\pi_j)}$,

$$\mathbb{E}_w [|\hat{Z} - \hat{Z}'|] = 2 \sum_{i=1}^{K-1} F_i (1 - F_i) (\hat{Z}_{b,t,d}^{(\pi_{i+1})} - \hat{Z}_{b,t,d}^{(\pi_i)}), \quad (10)$$

which avoids the $K \times K$ pairwise difference matrix. The reported CRPS averages $\text{CRPS}_{b,t,d}$ over all windows, steps, and channels.

A.3.2 Distortion

Distortion measures the quality of the single best hypothesis in each prediction window:

$$\text{Distortion} = \frac{1}{B} \sum_{b=1}^B \min_k \sqrt{\frac{1}{TD} \sum_{t,d} (\hat{Z}_{b,t,d}^{(k)} - Z_{b,t,d})^2}. \quad (11)$$

This is the standard winner-takes-all measure used in multiple-choice learning [9; 25].

A.3.3 Voltage Safety Metrics

All safety metrics are computed over voltage channels, indexed as the third coordinate of the interleaved $[P, Q, V, \theta]$ layout. Let \mathcal{V} index (b, t, d) triples on voltage channels, and $[V_{\min}, V_{\max}] = [0.95, 1.05]$ p.u.. The ground-truth violation event is $Y_{b,t,d} = \mathbf{1}\{V_{b,t,d} \notin [V_{\min}, V_{\max}]\}$ and the per-scenario indicator is $\hat{Y}_{b,t,d}^{(k)} = \mathbf{1}\{\hat{V}_{b,t,d}^{(k)} \notin [V_{\min}, V_{\max}]\}$. The per-scenario violation magnitude is

$$\delta_{b,t,d}^{(k)} = \max(0, V_{\min} - \hat{V}_{b,t,d}^{(k)}) + \max(0, \hat{V}_{b,t,d}^{(k)} - V_{\max}). \quad (12)$$

The three voltage safety metrics are then

$$\text{Safety_mBrier} = \frac{1}{|\mathcal{V}|} \sum_{(b,t,d) \in \mathcal{V}} \sum_k w_{b,d}^{(k)} (\hat{Y}_{b,t,d}^{(k)} - Y_{b,t,d})^2, \quad (13)$$

$$\text{NECV} = \frac{1}{|\mathcal{V}|} \sum_{(b,t,d) \in \mathcal{V}} \sum_k w_{b,d}^{(k)} \delta_{b,t,d}^{(k)}, \quad (14)$$

$$\text{CVaR}_{0.1} = \frac{1}{|\mathcal{V}|} \sum_{(b,t,d) \in \mathcal{V}} \frac{1}{\lceil 0.1K \rceil} \sum_{k \in \mathcal{T}_{0.1}(b,t,d)} \delta_{b,t,d}^{(k)}, \quad (15)$$

where $\mathcal{T}_{0.1}(b, t, d)$ selects the $\lceil 0.1K \rceil$ scenarios with the largest $\delta^{(k)}$ at (b, t, d) . The tail average for $\text{CVaR}_{0.1}$ uses uniform weights, matching the discrete CVaR estimator of [38]; weighting the tail by $w^{(k)}$ would suppress low-probability extreme scenarios and contradict the risk-averse intent.

Estimator choice for Safety_mBrier. The per-scenario form in Eq. (13) differs from the standard Brier on the weighted violation probability $\bar{Y}_{b,t,d} = \sum_k w_{b,d}^{(k)} \hat{Y}_{b,t,d}^{(k)}$ by a non-negative scenario-disagreement term, and reduces to the standard Brier in the deterministic limit. We retain the per-scenario form because grid contingency screening consumes scenarios individually rather than as a single aggregate violation probability. Each scenario is matched to a concrete remedial-action plan, so the operationally relevant quantity is the average forecast quality across scenarios as they are screened, not the calibration of the aggregate. A forecasting model whose mean violation probability is calibrated but whose scenarios disagree is operationally worse than one whose scenarios agree at the same mean, because the disagreement leaves the operator without a clear contingency to act on. The estimator is also unbiased on K weighted scenarios.

Interpretation. Safety_mBrier assesses *detection* (does the forecaster know when violations occur), NECV assesses *average severity*, and CVaR_{0.1} assesses *tail severity*. A forecaster can score well on CRPS while scoring poorly on these metrics if it concentrates probability mass near the conditional mean and underestimates the tails of the voltage distribution.

A.4 Bus Type Convention

Each bus is classified into one of three structural types:

Type	Name	Known (input)	Solved (output)
1	Slack (reference)	V, θ	P, Q
2	PV (generator)	P, V	Q, θ
3	PQ (load)	P, Q	V, θ

For PQ buses (the majority in all PowerPhase networks), P and Q are the exogenous inputs to the power-flow solver and V, θ are the physical responses. This structural asymmetry motivates the causal $P, Q \rightarrow V, \theta$ bridge in PowerForge (§4).

A.5 Train / Validation / Test Splits

All six PowerPhase networks share the same temporal split applied to the 70,176-step record (2015-01-01 to 2016-12-31 at 15-minute resolution):

Split	Period	Purpose
Train	2015-01-01 to 2016-06-30	Model training
Validation	Last 10 windows of train	Checkpoint selection
Test	2016-07-01 to 2016-12-31	Final evaluation

Test evaluation uses rolling-origin testing with 10 prediction windows of length $T_p = 96$ (one day). Each window uses a context of $T_h = 672$ steps (seven days) immediately preceding the prediction horizon. All reported metrics are averaged over these 10 windows and three random seeds.

B PowerForge Architecture

B.1 Anchor-Delta Details

The reference Z^{ref} in Eq. (4) is computed from the last $S \times L$ input steps reshaped into S non-overlapping daily segments of length $L = 96$, with $S = 7$ covering one week. The query X_c^{query} is the last $Q = 8$ steps of the input, and the key for segment s is the last Q steps of that segment. The Pearson correlation ρ between query and key is computed per channel with an $\epsilon = 10^{-8}$ stabiliser on the variance, and the temperature in the softmax is $\tau = 0.5$.

The reference day is tiled to match the input and prediction lengths, giving $Z_{\text{input}}^{\text{ref}}$ and $Z_{\text{future}}^{\text{ref}}$. The model consumes $x - Z_{\text{input}}^{\text{ref}}$ as input and emits residuals $\hat{\delta}$, recovered as $\hat{y} = \hat{\delta} + Z_{\text{future}}^{\text{ref}}$. For θ channels, both bias-correction differences and recovered values are wrapped to $[-\pi, \pi]$ via $\text{atan2}(\sin, \cos)$ to handle angular discontinuity.

A bias-correction term, the mean residual $x - Z_{\text{input}}^{\text{ref}}$ over the last $W = 8$ input steps, is added to both $Z_{\text{input}}^{\text{ref}}$ and $Z_{\text{future}}^{\text{ref}}$ before forming the residual. This absorbs slow drift between the periodic reference and the most recent observations. For θ channels, all reference and residual differences in this subsection are wrapped via $\text{atan2}(\sin, \cos)$, with full details in Appendix B.2.

B.2 Type-Specific Heads

Each per-type head consumes the fused state $h_c^{(m)} = h_c + e_m$ and emits a residual prediction $\delta_c^{(m)}$ over the T_p -step horizon.

P and Q heads. The P and Q heads are unbounded and parameterised as

$$\delta_c^{(m)} = \mu_c^{(m)} + \sigma_c^{(m)} \epsilon^{(m)}, \quad (16)$$

where $\mu_c^{(m)}$ is a linear projection of the fused state, $\sigma_c^{(m)}$ is a softplus-activated projection, and $\epsilon^{(m)}$ is a per-scenario noise vector. The default distribution is $\epsilon^{(m)} \sim \mathcal{N}(0, 1)$ resampled per batch, with a Student- t alternative ($\nu = 3$) also supported. The noise term acts as a stochastic regulariser rather than the source of scenario diversity. Diversity across the m axis is driven by the M learnable scenario embeddings $\{e_m\}$, which differentiate the branches at the input of the head, and is preserved by the pointwise sorting step in Section 4.5 that assigns each branch to a quantile level.

V and θ heads. The V head passes a learned projection $v_c^{(m)}$ through a tanh gate scaled by a learnable per-type magnitude Δ_V ,

$$\delta_{V,c}^{(m)} = \Delta_V \cdot \tanh(v_c^{(m)}), \quad (17)$$

with Δ_V initialised at 0.05 and floored at 10^{-4} . The initialisation reflects the operationally narrow voltage band around 1.0 p.u., and the floor prevents the gate from collapsing to zero during training. The θ head uses the same tanh-gate form with a fixed $\Delta_\theta = \pi$. Both gates structurally bound the residual without an explicit penalty.

Angular wrapping. For θ channels, both the bias-correction differences in Appendix B.1 and the recovered absolute predictions $\hat{y}_\theta = \hat{\delta}_\theta + Z_{\text{future},\theta}^{\text{ref}}$ are wrapped to $[-\pi, \pi]$ via $\text{atan2}(\sin, \cos)$ to handle the discontinuity at $\pm\pi$.

B.3 Channel Encoder

The channel encoder maps the input history $x \in \mathbb{R}^{B \times T \times C}$ into a per-channel representation $h \in \mathbb{R}^{B \times C \times H}$ through three additive sources of information.

Multi-scale temporal backbone. Each channel is processed independently by a shared temporal encoder. The raw signal and three 1-D convolutional filters with kernel sizes $k \in \{5, 25, 97\}$ extract features at 1.25-hour, 6.25-hour, and 1-day receptive fields at 15-minute resolution. Their outputs are concatenated along the feature axis and projected to dimension H through a two-layer GELU MLP. A per-channel scale token, obtained by passing the mean absolute value of each channel through a small MLP, is added to provide scale awareness across heterogeneous variable types. The result is layer-normalised with dropout 0.1.

Node, variable, and calendar features. Each channel additionally carries a learned node embedding ($d_{\text{node}} = 8$) and a variable-type embedding ($d_{\text{var}} = 2$). These two embeddings are concatenated and projected to dimension H , then added to the backbone output. They provide positional identity (which bus) and type identity (which of P, Q, V, θ). Calendar features (time of day, day of week) are averaged over the input window, projected to dimension H , and added as a shared offset across channels.

B.4 Training Objective Details

B.4.1 Full Loss Formulation

The total training loss is

$$\mathcal{L} = \mathcal{L}_{\text{OQ}} + \lambda_V \mathcal{L}_{\text{phys},V} + \lambda_\theta \mathcal{L}_{\text{phys},\theta} + w_{\text{width}} \mathcal{L}_{\text{width}} + w_{\text{jitter}} \mathcal{L}_{\text{jitter}} + \mathcal{L}_{\text{adapt}} + \mathcal{L}_{\text{Beta}} + w_{\text{gate}} \mathcal{L}_{\text{gate}}. \quad (18)$$

The Beta-prior term $\mathcal{L}_{\text{Beta}}$ keeps the learnable $\text{Beta}(\alpha, \beta)$ that parameterises τ_m close to its initial mean and scale, with weights 5×10^{-3} and 10^{-3} respectively. The gate term $\mathcal{L}_{\text{gate}}$ is an ℓ_2 penalty on the V/θ pre-backbone context gates toward their initialisation, with $w_{\text{gate}} = 2 \times 10^{-4}$.

B.4.2 Ordered-Quantile Loss (\mathcal{L}_{OQ})

Given M hypotheses and quantile levels $\tau_1 < \dots < \tau_M$ adapted during training through a learnable Beta-base law, the hypotheses are sorted along the scenario axis per channel and a pinball loss is applied:

$$\mathcal{L}_{\text{OQ}} = \frac{1}{BMT_p C} \sum_{b,m,t,c} \rho_{\tau_m}(Z_{b,t,c} - \hat{Z}_{b,t,c}^{(m)}), \quad (19)$$

where $\rho_\tau(u) = u(\tau - \mathbf{1}\{u < 0\})$ and $\hat{Z}^{(m)}$ is the m -th sorted hypothesis.

B.4.3 Physics Regularisation ($\mathcal{L}_{\text{phys}}$)

$\mathcal{L}_{\text{phys},V}$ applies a smooth- L_1 penalty toward zero on the voltage residual $\delta_{c,t}^{(m)}$ normalised by the learnable scale Δ_V (detached during this computation). This encourages voltage residuals to stay small relative to the gate width. $\mathcal{L}_{\text{phys},\theta}$ penalises the wrapped temporal difference $|\text{wrap}_{[-\pi,\pi]}(\hat{\theta}_{c,t+1}^{(m)} - \hat{\theta}_{c,t}^{(m)})|$, which prevents $\pm\pi$ jumps from being scored as oscillation. Both are averaged over scenarios, time, and channels of the relevant variable type. Default weights are $\lambda_V = 0.05$ and $\lambda_\theta = 0.01$.

B.4.4 Auxiliary Regularisers

Quantile width. $\mathcal{L}_{\text{width}}$ caps the inter-quantile spread between two reference quantile levels (default $\tau_{\text{low}} = 0.1$ and $\tau_{\text{high}} = 0.9$, taken as the closest hypotheses on the learned grid) at γ times a per-window per-channel target standard deviation $\sigma_{b,c}$:

$$\mathcal{L}_{\text{width}} = \frac{1}{BT_p C} \sum_{b,t,c} \text{ReLU}\left(\frac{|\hat{Z}_{b,t,c}^{(\text{high})} - \hat{Z}_{b,t,c}^{(\text{low})}|}{\gamma \sigma_{b,c}} - 1\right), \quad (20)$$

with $\gamma = 1.0$ and $w_{\text{width}} = 0.002$. The relative form prevents per-channel scale heterogeneity from biasing the penalty.

Temporal jitter. $\mathcal{L}_{\text{jitter}}$ discourages step-to-step oscillation of the median-centred quantile fan. After subtracting the median quantile, the temporal differences of the remaining quantiles are normalised by a per-window per-channel target standard deviation and averaged. The median itself is masked from the average. Default weight is $w_{\text{jitter}} = 0.001$.

Adaptive variable weights. A learnable vector $\omega \in \mathbb{R}^4$ scales the loss contribution of each variable type. It is initialised from the inverse per-type volatility on the first 40 training batches and clamped to $[0.3, 3.0]$. An ℓ_2 penalty with weight $w_{\text{adapt}} = 2 \times 10^{-4}$ regularises ω toward unity.

C Training and Implementation

C.1 Hyperparameters

Table 4 lists the main hyperparameters used across all PowerPhase networks.

Table 4: PowerForge hyperparameters (shared across all six PowerPhase networks unless noted otherwise).

Group	Parameter	Value
Architecture	Hidden dimension H	128
	Backbone kernel sizes	{5, 25, 97}
	Segment length	96
	Global tokens K	64
Embeddings	Node embedding dim	8
	Variable embedding dim	2
	Backbone dropout	0.1
Decoder	Number of hypotheses M	16
	Causal bridge scale init	1.0
	Scenario scoring	linear head
Anchor	Number of segments S	7
	Attention query length	8
	Attention temperature τ	0.5
Training	Objective mode	ordered-quantile
	Quantile levels	linspace(0.05, 0.95, 16)
	Learning rate	10^{-3}
	Weight decay	10^{-6}
Loss weights	Physics voltage λ_V	0.05
	Physics angle λ_θ	0.01
	Width regulariser	0.002
	Jitter regulariser	0.001
	Adaptive weight reg	2×10^{-4}
V/θ gate	Voltage Δ_V init	0.05
	Angle scale	π (fixed)
Input	Context length	672 steps
	Use full history	True

Table 5: Per-network training batch size for PowerForge.

Network	Batch size
ACTIVSg 500	32
PEGASE 1354	32
Polish 2383	16
PEGASE 2869	32
Polish 3120	32
PEGASE 9241	8

C.2 Implementation Details

C.2.1 Per-Network Batch Size

Batch sizes are chosen empirically per network to fit within the 96 GB GPU memory of the NVIDIA RTX PRO 6000 Blackwell GPU. Larger networks use smaller batches due to the linear scaling of activation memory with channel count. Table 5 reports the per-network values.

C.2.2 Train, Validation, and Test Splits

All six PowerPhase networks share the same temporal split applied to the 70,176-step record (2015-01-01 to 2016-12-31 at 15-minute resolution). The first 18 months form the training set, the last 6 months form the test set, and the final 10 windows of the training period are reserved for validation. Test evaluation uses rolling-origin testing with 10 equally spaced prediction windows of length $T_p = 96$ (one day). Each window uses a context of $T_h = 672$ steps (seven days) immediately

preceding the prediction horizon. All reported metrics are averaged over these 10 windows and three random seeds.

Table 6: Probabilistic forecasting results on POWERPHASE across five grids. CRPS, Distortion, and MSE measure *fidelity*; Safety_mBrier, NECV, and CVaR_{0.1} measure *safety*. All values are mean \pm std over three seeds. **Bold**: best; underline: second best.

Grid	Model	Fidelity \downarrow			Safety \downarrow		
		CRPS	Distortion	MSE	Safety_mBrier	NECV	CVaR _{0.1}
500-bus	DeepAR	0.1156 \pm 0.0240	0.5537 \pm 0.1310	0.0049 \pm 0.0013	0.9519 \pm 0.0233	0.8220 \pm 0.2702	2.1753 \pm 0.6901
	ETS	0.0064 \pm 0.0000	0.0481 \pm 0.0000	0.0006 \pm 0.0000	0.0561 \pm 0.0002	0.0026 \pm 0.0000	<u>0.0116</u> \pm 0.0000
	TimeMCL	<u>0.0054</u> \pm 0.0003	<u>0.0118</u> \pm 0.0001	0.0003 \pm 0.0002	<u>0.0200</u> \pm 0.0200	0.0191 \pm 0.0191	0.1906 \pm 0.1907
	TimePrism	0.0077 \pm 0.0003	0.0195 \pm 0.0023	0.0004 \pm 0.0002	0.0221 \pm 0.0062	<u>0.0014</u> \pm 0.0008	2.9950 \pm 1.1445
	TACTiS-2	0.0057 \pm 0.0002	0.0139 \pm 0.0006	<u>0.0002</u> \pm 0.0000	0.0000 \pm 0.0000	0.0000 \pm 0.0000	0.0000 \pm 0.0000
	TempFlow	0.0144 \pm 0.0008	0.0679 \pm 0.0005	0.0004 \pm 0.0001	0.2740 \pm 0.0519	0.0075 \pm 0.0018	0.0332 \pm 0.0043
	Trans-TempFlow	0.0146 \pm 0.0006	0.0702 \pm 0.0011	0.0004 \pm 0.0001	0.2896 \pm 0.0581	0.0081 \pm 0.0024	0.0380 \pm 0.0100
	TimeGrad	0.0160 \pm 0.0011	0.0954 \pm 0.0092	0.0010 \pm 0.0002	0.7630 \pm 0.0192	0.0977 \pm 0.0122	0.3316 \pm 0.0358
	PowerForge (Ours)	0.0030 \pm 0.0008	0.0072 \pm 0.0019	0.0001 \pm 0.0000	0.0000 \pm 0.0000	0.0000 \pm 0.0000	0.0000 \pm 0.0000
	1354-bus	DeepAR	0.1214 \pm 0.0342	0.6547 \pm 0.1231	0.0071 \pm 0.0013	0.8139 \pm 0.0766	0.3411 \pm 0.2354
ETS		0.0088 \pm 0.0000	0.0500 \pm 0.0000	0.0007 \pm 0.0000	0.1506 \pm 0.0007	0.0069 \pm 0.0000	0.0292 \pm 0.0000
TimeMCL		0.0097 \pm 0.0010	<u>0.0209</u> \pm 0.0002	0.0005 \pm 0.0000	0.0237 \pm 0.0123	0.0073 \pm 0.0055	0.0642 \pm 0.0548
TimePrism		0.0103 \pm 0.0017	<u>0.0216</u> \pm 0.0009	0.0026 \pm 0.0023	0.0403 \pm 0.0254	0.0270 \pm 0.0316	5.0594 \pm 2.9581
TACTiS-2		<u>0.0059</u> \pm 0.0001	0.0251 \pm 0.0010	<u>0.0004</u> \pm 0.0000	<u>0.0118</u> \pm 0.0006	<u>0.0008</u> \pm 0.0000	<u>0.0011</u> \pm 0.0000
TempFlow		0.0148 \pm 0.0073	0.0571 \pm 0.0274	0.0009 \pm 0.0004	0.2822 \pm 0.2348	0.0108 \pm 0.0086	0.0290 \pm 0.0242
Trans-TempFlow		0.0206 \pm 0.0007	0.0743 \pm 0.0003	0.0013 \pm 0.0001	0.4693 \pm 0.0352	0.0197 \pm 0.0027	0.0464 \pm 0.0042
TimeGrad		0.0109 \pm 0.0048	0.0945 \pm 0.0575	0.0023 \pm 0.0024	0.2496 \pm 0.1912	0.0493 \pm 0.0471	0.3581 \pm 0.2910
PowerForge (Ours)		0.0040 \pm 0.0003	0.0106 \pm 0.0003	0.0001 \pm 0.0000	0.0030 \pm 0.0000	0.0007 \pm 0.0000	0.0008 \pm 0.0000
2383-bus		DeepAR	0.0583 \pm 0.0261	0.4124 \pm 0.1674	0.0037 \pm 0.0038	0.5440 \pm 0.1632	0.0535 \pm 0.0465
	ETS	0.0111 \pm 0.0000	0.1513 \pm 0.0000	0.0058 \pm 0.0000	0.0352 \pm 0.0001	0.0029 \pm 0.0000	0.0099 \pm 0.0000
	TimeMCL	0.0070 \pm 0.0008	<u>0.0147</u> \pm 0.0016	0.0002 \pm 0.0000	0.0109 \pm 0.0068	0.0037 \pm 0.0054	0.0322 \pm 0.0547
	TimePrism	0.0096 \pm 0.0085	0.0250 \pm 0.0164	0.0015 \pm 0.0020	0.0294 \pm 0.0255	0.0061 \pm 0.0032	3.5007 \pm 1.1821
	TACTiS-2	0.0039 \pm 0.0000	0.0188 \pm 0.0000	<u>0.0002</u> \pm 0.0000	0.0036 \pm 0.0000	0.0005 \pm 0.0000	0.0007 \pm 0.0000
	TempFlow	0.0057 \pm 0.0001	0.0153 \pm 0.0026	0.0003 \pm 0.0000	<u>0.0032</u> \pm 0.0001	<u>0.0005</u> \pm 0.0000	<u>0.0005</u> \pm 0.0000
	Trans-TempFlow	0.0060 \pm 0.0002	0.0174 \pm 0.0002	0.0003 \pm 0.0000	0.0032 \pm 0.0000	0.0005 \pm 0.0000	0.0005 \pm 0.0000
	TimeGrad	0.0169 \pm 0.0016	0.1753 \pm 0.0826	0.0073 \pm 0.0038	0.5454 \pm 0.0505	0.1301 \pm 0.0638	0.8028 \pm 0.4729
	PowerForge (Ours)	<u>0.0042</u> \pm 0.0019	0.0084 \pm 0.0025	0.0001 \pm 0.0001	0.0010 \pm 0.0002	0.0004 \pm 0.0000	0.0004 \pm 0.0000
	2869-bus	DeepAR	0.1589 \pm 0.0028	0.7711 \pm 0.0301	0.0132 \pm 0.0019	0.9145 \pm 0.0083	0.8922 \pm 0.0319
ETS		0.0170 \pm 0.0000	0.1041 \pm 0.0000	0.0038 \pm 0.0000	0.0640 \pm 0.0005	0.0023 \pm 0.0000	0.0106 \pm 0.0000
TimeMCL		0.0235 \pm 0.0016	0.0608 \pm 0.0005	0.0039 \pm 0.0002	0.0228 \pm 0.0066	0.0130 \pm 0.0055	0.1271 \pm 0.0551
TimePrism		0.0222 \pm 0.0018	0.0593 \pm 0.0026	0.0036 \pm 0.0003	0.0862 \pm 0.0457	0.0018 \pm 0.0011	2.5224 \pm 1.3747
TACTiS-2		<u>0.0154</u> \pm 0.0001	0.0844 \pm 0.0038	<u>0.0036</u> \pm 0.0000	0.0069 \pm 0.0004	<u>0.0002</u> \pm 0.0000	0.0004 \pm 0.0000
TempFlow		0.0175 \pm 0.0019	0.0679 \pm 0.0040	0.0037 \pm 0.0001	<u>0.0062</u> \pm 0.0003	0.0003 \pm 0.0000	<u>0.0003</u> \pm 0.0000
Trans-TempFlow		0.0249 \pm 0.0069	0.0940 \pm 0.0238	0.0046 \pm 0.0007	0.3051 \pm 0.2633	0.0105 \pm 0.0095	0.0263 \pm 0.0228
TimeGrad		0.0269 \pm 0.0012	0.1707 \pm 0.0255	0.0123 \pm 0.0013	0.1201 \pm 0.0115	0.0162 \pm 0.0139	0.1361 \pm 0.1135
PowerForge (Ours)		0.0112 \pm 0.0004	0.0344 \pm 0.0011	0.0012 \pm 0.0001	0.0025 \pm 0.0000	0.0002 \pm 0.0000	0.0002 \pm 0.0000
3120-bus		DeepAR	0.1408 \pm 0.0148	0.7666 \pm 0.0842	0.0093 \pm 0.0017	0.7883 \pm 0.0160	0.6322 \pm 0.2054
	ETS	0.0180 \pm 0.0001	0.1954 \pm 0.0000	0.0075 \pm 0.0000	0.0987 \pm 0.0001	0.0069 \pm 0.0000	0.0225 \pm 0.0000
	TimeMCL	0.0092 \pm 0.0052	<u>0.0162</u> \pm 0.0044	0.0004 \pm 0.0004	0.1100 \pm 0.1071	0.0252 \pm 0.0242	0.2240 \pm 0.2385
	TimePrism	0.0083 \pm 0.0018	0.0213 \pm 0.0119	0.0013 \pm 0.0006	0.0579 \pm 0.0383	0.0043 \pm 0.0017	5.4230 \pm 3.2742
	TACTiS-2	<u>0.0043</u> \pm 0.0000	0.0297 \pm 0.0001	<u>0.0002</u> \pm 0.0000	0.0428 \pm 0.0006	0.0033 \pm 0.0001	0.0070 \pm 0.0000
	TempFlow	0.0056 \pm 0.0001	0.0178 \pm 0.0001	0.0003 \pm 0.0000	0.0188 \pm 0.0003	0.0033 \pm 0.0000	0.0035 \pm 0.0000
	Trans-TempFlow	0.0054 \pm 0.0002	0.0175 \pm 0.0006	0.0003 \pm 0.0000	<u>0.0184</u> \pm 0.0004	<u>0.0032</u> \pm 0.0000	<u>0.0034</u> \pm 0.0000
	TimeGrad	0.0123 \pm 0.0069	0.1295 \pm 0.0503	0.0035 \pm 0.0039	0.4234 \pm 0.1359	0.0887 \pm 0.0508	0.5695 \pm 0.2468
	PowerForge (Ours)	0.0038 \pm 0.0011	0.0076 \pm 0.0010	0.0001 \pm 0.0000	0.0068 \pm 0.0000	0.0025 \pm 0.0000	0.0025 \pm 0.0000

C.2.3 Optimisation and Checkpointing

PowerForge is trained with Adam at learning rate 10^{-3} and weight decay 10^{-6} , for up to 200 epochs per network. Validation loss is computed on the held-out validation windows after each epoch, and the checkpoint with the lowest validation loss is used for evaluation. The learning rate is halved by ReduceLROnPlateau when validation loss plateaus.

C.2.4 Baseline Configurations

Deep baselines (DeepAR, TempFlow, Transformer-TempFlow, TimeGrad, TACTiS-2, TimeMCL, TimePrism) follow their GluonTS [1] or original-release reference implementations. We use each baseline’s default optimiser, learning rate schedule, and training epoch budget as specified in its

reference codebase, with TACTiS-2 trained on its first stage only due to compute constraints at our scale. We apply the same train, validation, and test splits as PowerForge (Appendix C.2.2). ETS is fitted per channel by maximum likelihood on CPU.

D Full Results on the Five Main Grids

Table 6 reports six metrics on every model across the five main PowerPhase grids, extending the three-grid scoreboard in Table 2.

The pattern from the representative grids holds across the full set. PowerForge attains the best score on every metric on PEGASE 1354, PEGASE 2869, and Polish 3120, the best Distortion, Safety_mBrier, and CVaR_{0.1} on Polish 2383 with CRPS within seed variance of the strongest baseline, and ties with TACTiS-2 on Safety_mBrier and CVaR_{0.1} at ACTIVSg 500 where both achieve zero violations. The two intermediate grids not shown in the main text (PEGASE 1354, PEGASE 2869) follow the same ordering.

E Evaluation at 36,964 Channels: PEGASE 9241

This appendix evaluates PowerForge at the upper end of the PowerPhase scale, on PEGASE 9241 (36,964 channels). The five-grid evaluation in Section 5.2 characterises PowerForge against the full eight-baseline panel. Here we extend the comparison at maximum scale to four baselines spanning three families: TimeMCL and TimePrism (scenario-based), Transformer-TempFlow (conditioned normalising flow), and ETS (statistical reference). DeepAR, TimeGrad, TACTiS-2, and TempFlow are not included in this comparison. TempFlow’s behavior closely tracks Trans-TempFlow on the five main grids. PowerForge, TimePrism, TimeMCL, ETS and Transformer-TempFlow are evaluated with three random seeds {22, 42, 3142}.

Table 7: Probabilistic forecasting results on PEGASE 9241 (36,964 channels). CRPS and Distortion measure *fidelity*; Safety_mBrier and CVaR_{0.1} measure *safety*. Values are mean±std over three seeds. **Bold**: best; underline: second best.

Model	<i>Fidelity</i> ↓		<i>Safety</i> ↓	
	CRPS	Distortion	Safety_mBrier	CVaR _{0.1}
ETS	0.0413 ± 0.0001	0.4515 ± 0.0009	0.1361 ± 0.0001	0.0395 ± 0.0001
TimeMCL	0.0349 ± 0.0129	0.0629 ± 0.0030	0.2326 ± 0.3072	0.4726 ± 0.4843
TimePrism	<u>0.0112</u> ± 0.0029	<u>0.0427</u> ± 0.0046	0.0506 ± 0.0393	1.5350 ± 0.3220
Trans-TempFlow	0.0224 ± 0.0019	0.0748 ± 0.0039	<u>0.0087</u> ± 0.0013	<u>0.0029</u> ± 0.0001
PowerForge (Ours)	0.0077 ± 0.0008	0.0185 ± 0.0024	0.0021 ± 0.0000	0.0023 ± 0.0000

PowerForge attains the best score on every metric. Two observations transfer the pattern of Section 5.2 to the maximum-scale setting. First, the safety–fidelity trade-off remains visible: TimePrism is competitive on CRPS (0.0112) but its CVaR_{0.1} degrades to 1.535, indicating that its hypothesis spread covers infeasible voltage states with substantial probability. Trans-TempFlow follows the inverse pattern observed at 3120-bus, with strong safety scores but weaker fidelity than PowerForge. Second, ETS scales to 36,964 channels through per-channel CPU fitting and provides a non-trivial statistical reference, but its CRPS and Distortion sit an order of magnitude above the deep baselines, consistent with the pattern observed on the five main grids.

F Additional Safety Analyses

F.1 Additional Qualitative Comparison: PEGASE 1354

Figure 4 reports the same three-row qualitative comparison on PEGASE 1354 (5,416 channels). PowerForge produces a compact hypothesis set that tracks the diurnal trajectory, TimePrism recovers the shape with a wider spread, and TACTiS-2’s median tracks the morning trough on this nominal-band bus while individual samples retain high-frequency jitter. The qualitative ordering across

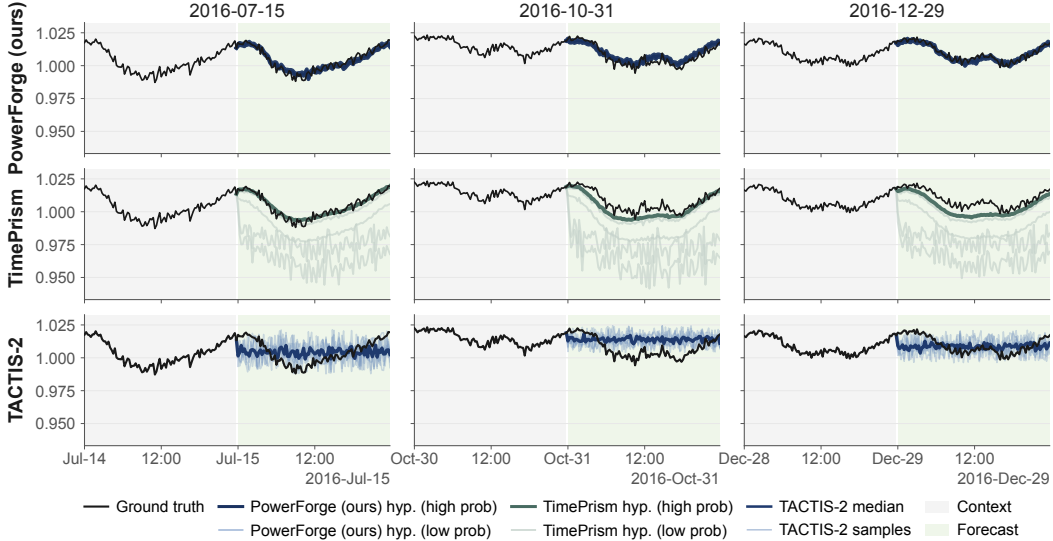


Figure 4: Voltage forecasts on PEGASE 1354 (5,416 channels) for a single bus across three test windows. The three-row structure mirrors Figure 3. This bus operates in the nominal voltage band with a morning diurnal trough, in contrast to the boundary-crossing evening-trough bus in Figure 3. TACTiS-2’s median tracks the morning dip across all three windows while samples retain high-frequency jitter, and the qualitative ordering across forecasters is preserved relative to the Polish 2383 case.

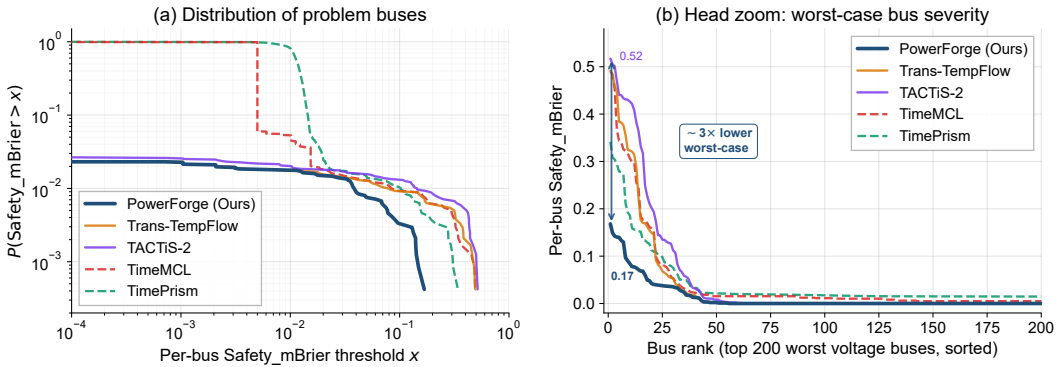


Figure 5: Bus-level aggregate voltage safety on Polish 2383 (9,532 channels), computed as per-bus Safety_mBrier averaged across all forecast scenarios, time steps, and ten test windows. **(a)** Survival function of per-bus Safety_mBrier. PowerForge, Trans-TempFlow, and TACTiS-2 (solid) keep $\sim 97\%$ of 2,383 buses below any non-trivial threshold, while TimeMCL and TimePrism (dashed) place violation probability on nearly all buses. **(b)** Top-200 worst buses, sorted by severity. PowerForge top-1 bus 0.17 vs 0.52 (TACTiS-2), an $\sim 3\times$ improvement on the hardest bus. ETS, DeepAR, and TimeGrad are omitted (full results in Table 6).

forecasters is preserved relative to the Polish 2383 case in the main text, although the per-step sample jitter of TACTiS-2 is more salient than its low-frequency flattening on this particular bus.

F.2 Bus-level aggregate distribution on Polish 2383

Section F.1 extends the channel-level analysis of Section 5.3 to PEGASE 1354. Here we complement the channel-level view with a network-level distributional analysis on Polish 2383, the grid used for the main qualitative figure. The per-bus Safety_mBrier (Figure 5) measures how often and how confidently each model places probability mass outside the $[0.95, 1.05]$ p.u. voltage band at each of the 2,383 voltage buses.

Panel (a): distribution of problem buses. The horizontal axis is a per-bus Safety_mBrier threshold x on log scale, and the vertical axis is the fraction of buses whose per-bus value exceeds x . Two regimes emerge. PowerForge, Trans-TempFlow, and TACTiS-2 (solid) sit near $y \approx 0.025$ even at very small x , meaning roughly 97% of buses are forecast cleanly and violations concentrate on a small problem set. TimeMCL and TimePrism (dashed) instead remain near $y = 1.0$ until $x \approx 10^{-2}$, indicating pervasive low-magnitude violations across almost all buses. This separation matches the safety-fidelity trade-off in Table 6.

Panel (b): worst-case bus severity. The horizontal axis is the rank of the worst 200 buses per model, sorted by descending per-bus Safety_mBrier. Among the three sparse-violation methods, PowerForge has top-1 bus severity 0.17 versus 0.49 (Trans-TempFlow) and 0.52 (TACTiS-2). PowerForge’s curve also stays consistently below the other four models across the full top-200 head.

Network-determined hard buses. The hard-bus set is largely shared across the three sparse-violation models. The top-50 problem buses overlap 100% between PowerForge and Trans-TempFlow, and 96% between PowerForge and TACTiS-2. Per-bus Safety_mBrier rankings across all 2,383 buses are also strongly correlated, with Spearman $\rho > 0.999$ between PowerForge and Trans-TempFlow and $\rho = 0.928$ between PowerForge and TACTiS-2. The hard-bus set is therefore largely determined by the forecasting task on this network rather than by individual model choices. PowerForge does not eliminate the hard-bus phenomenon, but reduces worst-case severity on the same network-determined set.

G Full Ablation Results on PEGASE 1354

Table 8: Ablation on PEGASE 1354 (5,416 channels), single seed. Δ is the relative CRPS change against the full configuration. Variants are ordered by descending CRPS impact. Lower is better for all metrics.

Variant	CRPS ↓	Δ	Distortion ↓	Safety_mBrier ↓	NECV ↓	CVaR _{0.1} ↓
Full PowerForge	0.00433	–	0.0110	0.00301	7.41e-4	7.52e-4
w/o anchor-delta	0.00797	+84%	0.0229	0.03042	8.09e-4	1.90e-3
w/o quantile regularisation	0.00594	+37%	0.0128	0.00310	7.41e-4	7.54e-4
w/o ordered-quantile (WTA)	0.00551	+27%	0.0155	0.00448	7.46e-4	8.71e-4
w/o physics regularisation	0.00550	+27%	0.0120	0.00308	7.39e-4	7.52e-4
w/o cross-type causal bridge	0.00530	+22%	0.0120	0.00307	7.40e-4	7.53e-4
w/o low-rank global mixer	0.00450	+4%	0.0154	0.00303	7.36e-4	7.42e-4

Table 8 extends the PEGASE 1354 ablation in Section 5.4 to the full PowerPhase metric suite (CRPS, Distortion, Safety_mBrier, NECV, CVaR_{0.1}) under a single random seed. The safety metrics identify anchor-delta as the dominant component for voltage-band feasibility, while the remaining variants leave Safety_mBrier, NECV, and CVaR_{0.1} close to the full-model baseline.